Biophysical Journal, Volume *120*

Supplemental information

Elastic wrinkling of keratocyte lamellipodia driven by myosin-induced contractile stress

Sunny S. Lou, Andrew S. Kennard, Elena F. Koslover, Edgar Gutierrez, Alexander Groisman, and Julie A. Theriot

Supplemental Mathematical Model

The following is a quantitative mechanical model for the lamellipodial wrinkling we observe, designed with the specific goal of calculating the dependence of the wrinkle wavelength on geometric and material properties of the lamellipodial F-actin network, such as its thickness and bending modulus. The mathematical relationship between these quantities is derived in the framework of elasticity theory, and is thus analogous to the relationships previously obtained for wrinkling in different systems (1, 2). The particular derivation given here is specific to the boundary conditions and constraints of the lamellipodium, which is attached to the substrate via a thin adhesive layer and cannot buckle below the substrate. Our derivation shows that, just as in the previously studied systems with wrinkles, an optimal wrinkling wavelength is selected and it is constrained from below by the resistance of the actin network to bending.

We model the F-actin cytoskeleton in the lamellipodium as a thin elastic sheet in the *xy*-plane with a thickness h, length L and width w (x- and y-dimensions) and elastic modulus E_t, and assume that myosin tension results in a compressive strain Ualong the x-axis direction (the direction parallel to the leading edge). The compressive strain is treated as being distributed continuously throughout the elastic sheet, with U corresponding to its integral across the sheet. This continuous strain represents the action of myosin motors acting as force dipoles that are scattered broadly within the sheet. Our model treats the lamellipodium near the leading edge only, neglecting two-dimensional effects that may arise due to higher concentrations of myosin motors further back from the leading edge.

We assume that, when there is no compression, the elastic sheet rests on the ventral membrane of the cell and that the sheet is attached to the ventral membrane by an array of springs, each representing an individual adhesion complex. These springs have an area density g, resulting in an effective substrate Young's modulus $E_c = k_s\, g$, where k_s is the stretch elasticity of an individual spring. A greater spring density g would thus result in a higher effective Young's modulus E_c. When the local distance between the wrinkled elastic sheet and the ventral membrane differs by ζ, it costs elastic energy of $E_c\, \zeta^2/2$ per unit area. We note that this physical picture is closely related to a previously described model for the wrinkling of a thin hard sheet resting on a semi-infinite soft elastic substrate (1). However, the deformation of the soft medium in such a model is spread over a depth proportional to the wavelength, yielding a vertical strain that scales as deformation amplitude over wavelength and an overall energy of deformation of the elastic substrate that scales as amplitude squared divided by the wavelength. By contrast, in our model, the cumulative energy of the springs is wavelength-independent and scales simply as the amplitude squared.

Furthermore, we expect the energetics of the actin sheet interacting with the surface to be highly asymmetric, with a stiff contact energy preventing the sheet from penetrating the ventral membrane and a softer energy of stretched springs due to displacement of the actin away from the ventral surface. Consequently we focus the subsequent discussion on periodic wrinkle patterns confined to the positive half-space ($\zeta > 0$).

For a periodic pattern of wrinkles with a wavenumber k along the *x*-axis and amplitude ζ_0,$\zeta = \zeta_0(1 - \cos(\mathrm{kx}))$, the bending energy is given by

$$F_b = \frac{1}{2} B \int \left(\frac{\partial^2 \zeta}{\mathrm{dx}^2}\right)^2 \mathrm{dxdy} = \frac{1}{4} \mathrm{BwLk}^4 \zeta_0^2,$$

where $B = \frac{1}{12} \frac{E_t h^3}{(1-\nu^2)}$ is the bending modulus of the thin sheet and $\nu$is its Poisson ratio. The energy of stretching of the springs is

$$F_c = \frac{1}{2} E_c \int \zeta^2 \mathrm{dxdy} = \frac{3}{4} E_c \mathrm{wL} \zeta_0^2.$$

The total energy per unit area is

$$\frac{F_t}{\mathrm{wL}} = \frac{1}{4}\left(3E_c \zeta^{2}{}_0 + \frac{1}{12} \frac{E_t h^3}{(1-\nu^2)} k^4 \zeta_0^2\right).$$

We now assume that the wrinkling relieves the x-axis strain, *U*, such that

$$U = \frac{1}{L} \int \frac{1}{2} \left(\frac{\partial \zeta}{\mathrm{dx}}\right)^2 \mathrm{dx} = \frac{(\zeta_0 k)^2}{4}.$$

Plugging this expression into the equation for the total energy per unit area, we obtain

$$\frac{F_t}{\mathrm{wL}} = U\left(3\,E_c/k^2 + \frac{1}{12} \frac{E_t h^3}{(1-\nu^2)} k^2\right) = U\left(\frac{3E_c \lambda^2}{(2\pi)^2} + \frac{1}{12} \frac{(2\pi)^2 E_t h^3}{(1-\nu^2)} \frac{1}{\lambda^2}\right).$$

The free energy is proportional to a sum of two expressions, one with λ^2in the numerator and the other with λ^2in the denominator. Therefore, it is clear that there is an optimum value of the wavelength minimizing the free energy. This value (found by differentiating the equation with respect to λ and equating the derivative to zero) is

$$\lambda = 2\pi \left(\frac{h^3}{12(1-\nu^2)} \frac{E_t}{3E_c}\right)^{1/4} \propto \left(h^3 \frac{E_t}{E_c}\right)^{1/4}.$$

Importantly, E_t scales with the bending modulus, *B*, and E_c scales with adhesion density, g. The optimum wavelength is an inverse function of g and, as in previous models of elastic wrinkling, a direct function of *B*. The selection of the optimum wavelength arises from a balance between the energy associated with bending the elastic sheet and that required to stretch adhesive bonds. In the elastic model described here, both the stretching and the bending energy depend on the squared amplitude of the wrinkling deformation, and this squared amplitude varies in proportion to the applied strain U. Since both energy terms have the same dependence on the strain, the optimal wavelength is strain-independent, and increasing compression should simply raise the magnitude of the wrinkles without varying their wavelength. Our experimental data is consistent with this prediction (Fig. S4e). While a strain-dependent wavelength could be derived from other models where the constraint keeping the actin sheet attached to the ventral surface is not linearly elastic in nature, we chose to focus here on the simplest model reproducing the observed behavior.

Comparison to experimental data

Note that our model predicts a $1/4$ power law scaling relationship between λ and E_t and between λ and E_c. This prediction is difficult to test experimentally, because the bending modulus of the actin sheet and stretching modulus of the molecular bonds between the substratum and the actin network (that the adhesion complexes are part of) cannot be directly measured. Nonetheless, if we make the rough assumption that the actin sheet behaves similarly to an in vitro entangled cross-linked network, where E_t has been shown to scale with actin filament density to the power 2.2 (3), our model would predict

$$\lambda \propto (actin\ density)^{2.2/4} = (actin\ density)^{0.55}$$

i.e. a 50% decrease in actin density should result in a 32% decrease in wavelength. When plotted together with our experimental data, a power law of 0.55 shows reasonable agreement (Fig. 6j). It should be noted, however, that the perturbations employed in this study (pH changes and latrunculin application) may in principle affect other aspects of the system, such as the thickness of the actin sheet. If the latter effect was to dominate, a scaling of wavelength with phalloidin density to the 0.75 power would be expected. Given the substantial variability of measurements between cells, a more definitive comparison between model and experiment is precluded.

Finally, the stability of the periodic wrinkling patterns discussed here depends on the precise boundary conditions and the form of the contact energy preventing penetration of the elastic sheet below the ventral surface. The periodic wrinkling pattern would be destabilized if the springs were allowed to break beyond a certain cutoff height, as seems likely given the large amplitude of wrinkling at large distances from the cell leading edge. Because the breaking of adhesions increases the vertical stress on neighboring adhesions caused by the buckled actin sheet, this adhesion breaking could spread like a fracture, leading to delamination of the sheet. In this scenario, a periodic wrinkled pattern is inherently unstable and, given sufficient time, the actin network would fully detach from the ventral membrane (or the ventral membrane would detach from the substratum) to make a single large bump above the lamellipodium. A stable wrinkling pattern requires some elastic constraint to prevent the formation of such a large bump, and we therefore hypothesize that the periodic wrinkle pattern is maintained by the intact adhesions at the leading edge, where the amplitude of wrinkles is small. Unlike the simple one-dimensional model we formulated and analyzed above, the actual actin network is two-dimensional and, within 30-60 s, it moves all the way back towards the cell body (in the framework of the moving cell), which may not allow enough time for catastrophic delamination. The simple model described here thus contains the fundamental physical ingredients leading to the selection of an optimal wavelength for periodic wrinkling and predicts the character of the dependence of this wavelength on the bending modulus of the actin sheet and the density of the adhesion complexes.

An alternate explanation for stable wrinkle pattern formation could be a catch-bond response in adhesions near the wrinkle troughs, with adhesion binding strength increasing under higher stress. Such a stress response at the molecular level could prevent large-scale delamination that joins multiple wrinkles into a single large bump. However, a separate mechanism would then need to be postulated to explain delamination at the peaks of the wrinkles. A sufficiently high stress to break adhesions at the wrinkle peak would lead to concentration of even higher stresses in nearby adhesions, again triggering a propagating delamination. Maintaining a stable wrinkle pattern would

then require either spatially heterogeneous adhesion properties or time-dependent variation in the stresses and strains on the lamellipodial sheet as it moves backward from the leading edge, both of which lie outside the scope of the current work.

Supplemental Figures

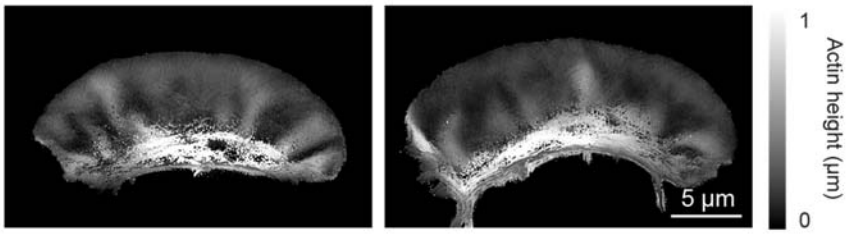

Figure S1 – Keratocyte fragments also form wrinkles (related to Figure 1).
Two example actin height maps of keratocyte fragments with wrinkles

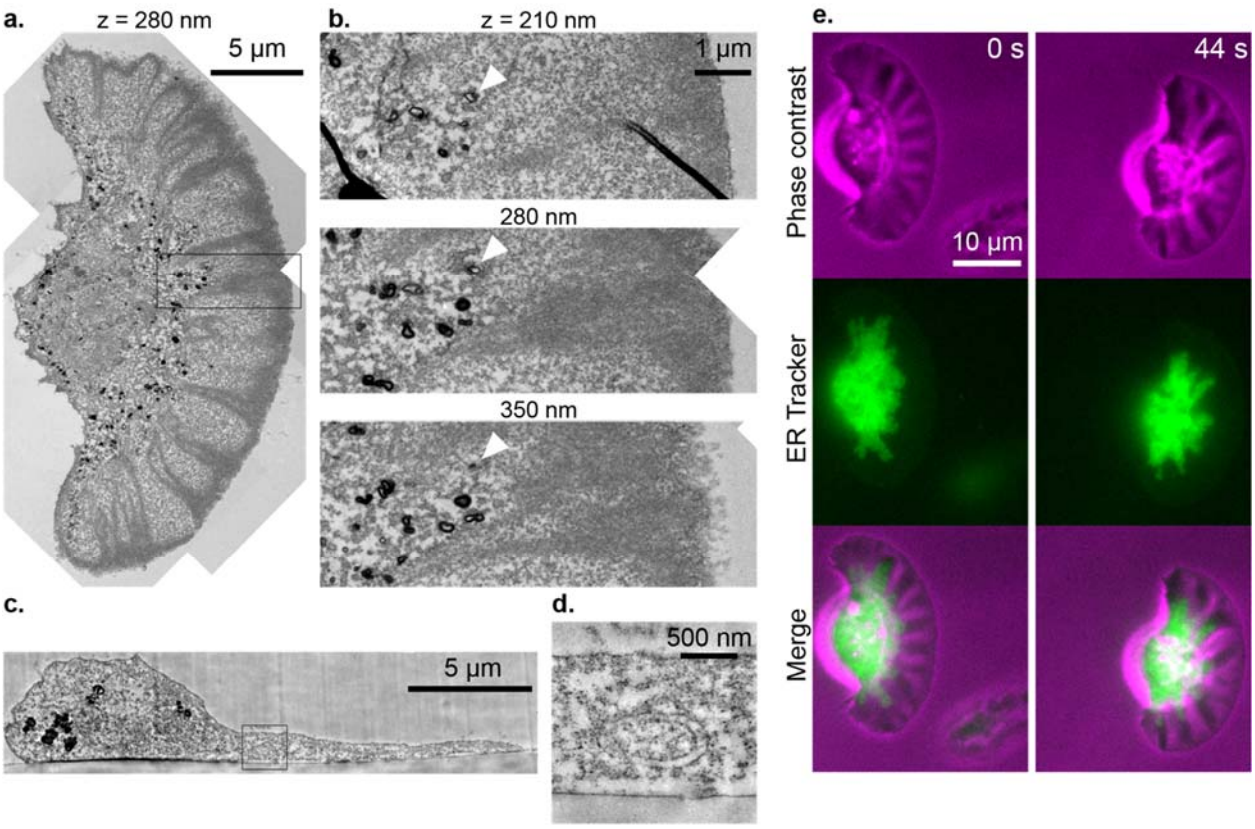

Figure S2 – Wrinkles open space in lamellipodium for vesicles and organelles (related to Figure 2).

a. Slice from an electron micrograph showing wrinkled actin structures in the lamellipodium and small membranous structures permeating underneath the lamellipodial wrinkles. Sections are taken parallel to the coverslip and z indicates the approximate distance from the coverslip
b. Inset of region boxed in (a), with the same region from sections immediately before and after the section shown in (a). The vesicles can be seen spanning multiple sections, and the position of the vesicles relative to the actin network suggests that they are below the actin network, at the back of the lamellipodial region.
c. A different section of the same cell shown in Fig. 2e, showing and object within the lamellipodial space.
d. Higher resolution view of the boxed region in (c), showing the presence of a membranous structure within the lamellipodium.

e. Stills from a timelapse movie of a keratocyte labeled with ER Tracker dye. IN these frames the endoplasmic reticulum penetrates into the taller regions of the lamellipodium, indicated by phase-dense regions (cf. Fig. 1b).

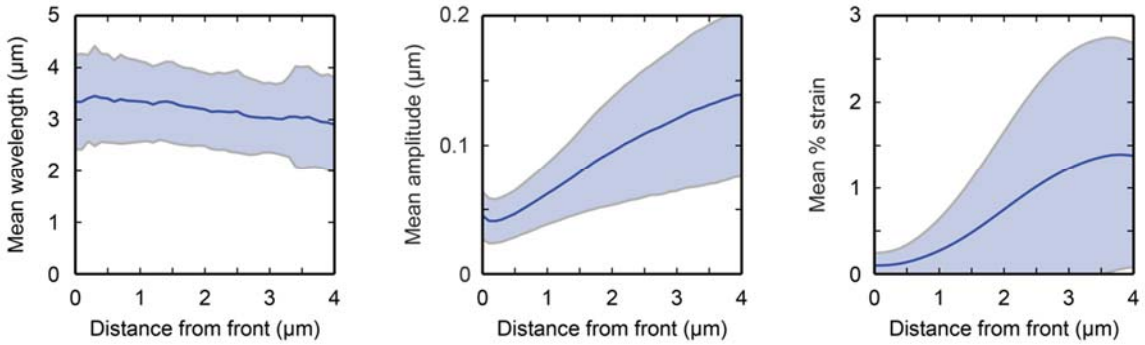

Figure S3 – Wrinkle properties vary with distance from the leading edge (related to Figure 3). Mean wavelength, amplitude, and strain measured in n = 168 cells at distances ranging from 0 to 4 μm in from the leading edge. Shaded area shows standard deviation.

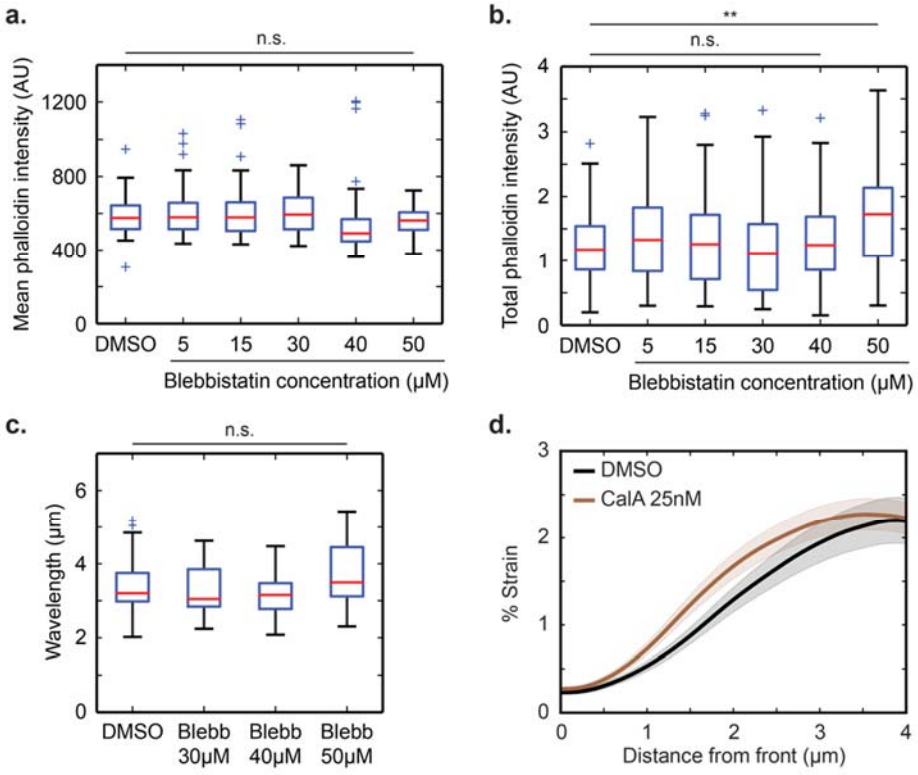

Figure S4 – Effect of blebbistatin and calyculin on wrinkle geometry (related to Figure 5).

a. Average phalloidin intensity per cell, normalized for cell area, for the indicated cell populations. N = 57, 95, 109, 76, 122, 108, respectively, for the conditions shown.

b. Total summed phalloidin intensity per cell for the indicated cell populations. Sample sizes are the same as in a.
c. Mean wavelength per cell measured 2.5μm from the leading edge for the indicated cell populations. N = 18, 24, 27, 20, respectively.
d. % strain as a function of distance from the leading edge measured in cell populations treated with calyculin compared with DMSO control. N = 59 for DMSO treatment; N = 80 for calyculin treatment.

n.s.: $p > 0.05$, **: $p < 0.01$ as measured by two-sample t-test.

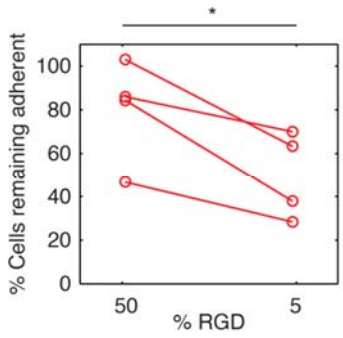

Figure S5 – Varying surface RGD affects cell adhesivity (related to Figure 6).
Cells plated on surfaces functionalized with 50% and 5% RGD were counted before and after a one-minute 500×g centrifugation of the inverted coverslip. Plotted is the % of cells remaining on the surface after centrifugation. Data points coming from the same batch of coverslip preparation are connected by a line (n = 4 batches). *: $p < 0.05$ as measured by a paired-sample t-test.

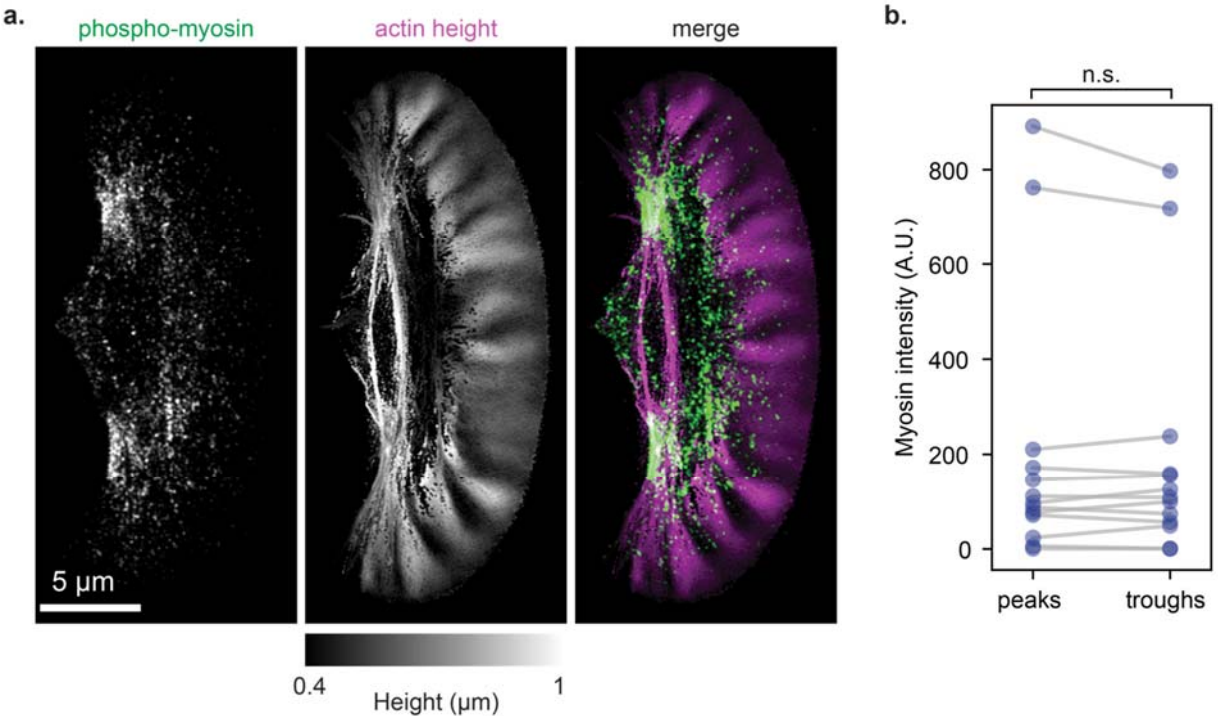

Figure S6 – Myosin localization does not correlate with wrinkle positions near the leading edge (related to Figure 6).

a. SIM image of a keratocyte showing phospho-myosin antibody staining and the height of the actin network based on phalloidin, as described in the Materials and Methods. Myosin puncta appear scattered throughout the lamellipodium.

b. Average phospho-myosin intensity in a 3µm deep by x 1.4µm wide region around each peak or trough in each cell. Paired data reflect the average intensity across all peaks or troughs in a single cell (n = 13 cells).

n.s.: not significant ($p > 0.5$, two-tailed paired t-test).

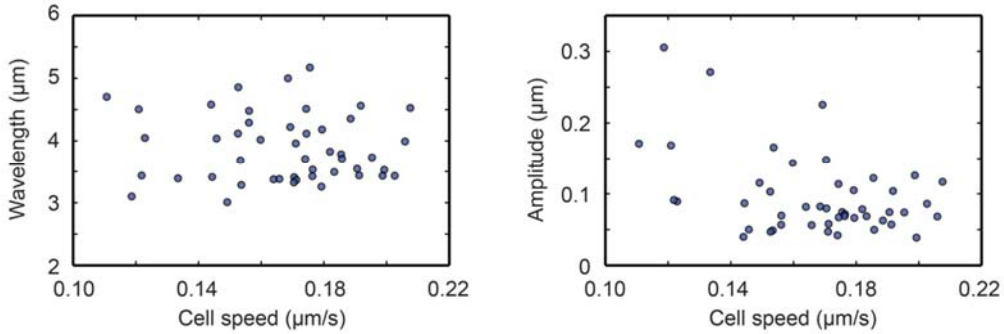

Figure S7 – Neither wavelength nor amplitude positively correlate with cell speed (related to Figure 6).

Correlation between cell speed and wavelength or amplitude is shown (n = 49 cells). Slower cells have more time for actin turnover.

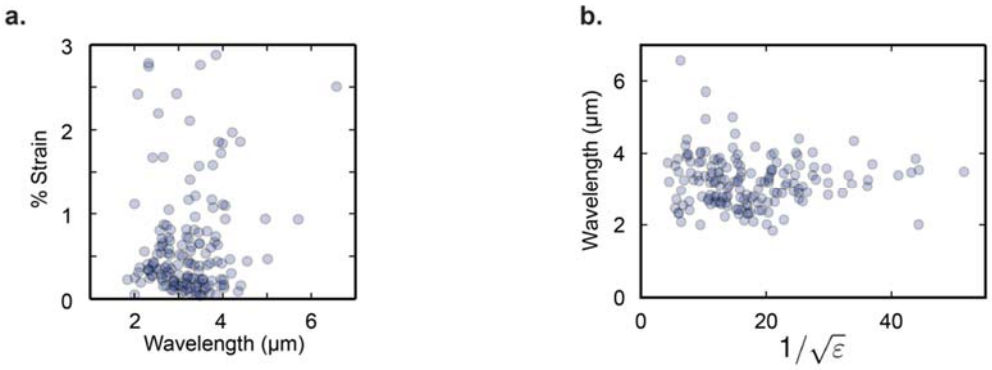

Figure S8 – Wavelength and effective strain are not correlated (related to Figure 6).
a. Wavelength plotted vs. % strain for 163 untreated cells.
b. Wavelength plotted vs. inverse square root of strain for same cells as in (a). cf. Supp. Ref. 4.

Supplemental Movie Legends

Movie S1 – 3D rendering of the actin cytoskeleton illustrates wrinkle geometry (related to Fig. 1)
3D rendering of the AF488-phalloidin-stained actin cytoskeleton in a representative cell as imaged by 3D structured illumination microscopy. Movie shows the rendering rotated around the x and z axes. This video corresponds to Fig. 1c.

Movie S2 – Live imaging of ventral membrane dynamics. (related to Fig. 1)
Time-lapse phase contrast and TIRF microscopy movie of the representative cell expressing membrane-localized EGFP-CAAX shown in Fig. 1f. Time stamp (upper right) is in the format minutes:seconds. Frames were acquired every 3 seconds for 3:21 minutes. Scale bar is 10 microns.

Movie S3 – Wrinkles allow endoplasmic reticulum to penetrate into the lamellipodium (related to Fig. S2)
Side-by-side views of phase contrast (magenta, left) and widefield fluorescence microscopy (green, center) of a representative cell whose endoplasmic reticulum is stained with the dye ER Tracker. The right panel shows the two channels merged together. As the wrinkle pattern changes over time, the infiltration of the ER into the lamellipodium follows the wrinkles. Frames were acquired every 4 seconds for 160 seconds. Scale bar is 10 μm. This video corresponds to Fig. S2e.

Movie S4 – Wrinkle positions over time in a motile cell (related to Fig. 4)
Time-lapse phase microscopy movie of a representative cell where wrinkle peaks as detected by our algorithm are continuously overlaid over the movie. Images were acquired with a widefield microscope. Time stamp (upper left) is in the format minutes:seconds. Frames were acquired every 2 seconds for 4 minutes. Scale bar is 10 microns. This video corresponds to Fig. 4c.

Supporting References

1. Groenewold, J. 2001. Wrinkling of plates coupled with soft elastic media. *Phys. A Stat. Mech. its Appl.* 298:32–45.

2. Cerda, E., and L. Mahadevan. 2003. Geometry and physics of wrinkling. *Phys. Rev. Lett.* 90:074302.

3. Mackintosh, F.C., J. Käs, and P.A. Janmey. 1995. Elasticity of semiflexible biopolymer networks. *Phys. Rev. Lett.* 75:4425.

4. Ideses, Y., V. Erukhimovitch, R. Brand, D. Jourdain, J. Salmeron Hernandez, U.R. Gabinet, S.A. Safran, K. Kruse, and A. Bernheim-Groswasser. 2018. Spontaneous buckling of contractile poroelastic actomyosin sheets. *Nat. Commun.* 9:2461.